Mechanical and damage fields ahead of a stationary crack in a creeping solid

Abubakker Sithick Basha A[a], Sivasambu Mahesh[a,*]

[a]*Department of Aerospace Engineering, Indian Institute of Technology Madras, Chennai, 600036 India.*

Abstract

The evolution of mechanical and damage fields, and the time to failure of material points ahead of a stationary crack in a compact tension specimen are computed using finite element simulations for a linear elastic/power law creeping material. These are compared with predictions obtained from fields based on two fracture mechanics based load-parameters: the steady-state C^*, and the time-corrected $C(t)$. The finite element calculations predict opening stress in the crack plane that are non-monotonic in the time interval $0 \leq t \leq t_1$, where t_1 denotes the time to transition from small-scale creep to extensive creep. This is in contradiction to the monotonic 'self-similar' decay of stress with time given by the $C(t)$ field. Consequently, damage rates and times to failure of material points ahead of a crack calculated using the finite element stress-field, and the $C(t)$-based stress-field diverge considerably. These observations suggest that the creep damage rates derived on the basis of self-similarly decaying opening stress fields may be severely inaccurate.

Keywords: fracture mechanics, creep crack, C^*-field, continuum damage

1. Introduction

Crack growth in a creeping body has been the subject of a large number of theoretical, computational and experimental studies extending at least over the

*Corresponding author

Email addresses: `ae13m001@smail.iitm.ac.in` (Abubakker Sithick Basha A), `smahesh@iitm.ac.in` (Sivasambu Mahesh)

past five decades [1]. The difficulty of obtaining a predictive model of creep crack growth owes as much to the complex spatiotemporal mechanical fields associated with a creep crack, as to the microscopic damage mechanisms underlying creep crack extension.

A relationship between the creep crack growth rate $\dot{a}$ and the load parameter for secondary creep, C^*, was derived by Kubo et al. [2]. Taking the Hutchinson-Rosengren-Rice (HRR) [3, 4] field to represent the distribution of stress ahead of a creep crack, and assuming that the damage rate is proportional to power b_1 of the local normal stress, Kubo et al. [2] found that $\dot{a} \propto C^{*b_1/(n+1)}$, where n denotes the Norton exponent. In their model, a material point located a microstructural distance ρ_s fails at the time when its damage parameter reaches a value of 1. A similar scaling was obtained later by Hui and Banthia [5], including the effect of a critical stress for void nucleation. Using a critical strain based failure criterion at a microstructural distance ahead of the crack tip, Riedel and Wagner [6] obtained the scaling $\dot{a} \propto C^{*n/(n+1)}$.

The above scaling has seen mixed success in capturing experimentally measured dependence of $\dot{a}$ with C^*. In Cr-Mo steel, Riedel and Wagner [7] found excellent correlation between $\dot{a}$ and $C^{*n/(n+1)}$ over a range of temperatures. Further experimental evidence of correlation was offered by Riedel and Detampel [8]. Later works, due to Maas and Pineau [9], Bensussan et al. [10], and Piques et al. [11], however, have reported marked deviation of the experimentally measured $\dot{a}$ and C^* from the simple power-law relationship predicted by the models. Maas and Pineau [9] and Bensussan et al. [10] suggested that the correlation observed in some preceding works may have been spurious in tests wherein the C^* parameter is determined from the experimental load line displacement. They reasoned that at high crack growth rates, the load line displacement simply reflects crack propagation, which leaves the experimental approach erroneously correlating $\dot{a}$ with itself.

Even when C^* is not computed from the load line displacement, a number of reasons may underlie the breakdown of the simple power-law relationship between $\dot{a}$ and C^*. The most prominent among them is the deviation of the crack-tip mechanical fields from the HRR field. Riedel [12] suggested that the loading parameter employed must be the stress intensity factor K if the specimen deformation is predominantly elastic, the J-integral if the specimen deformation is predominantly plastic with creep confined to a small region, the C_h^* integral when the bulk of the specimen is under primary or tertiary creep, and the C^* integral when the specimen is predominantly under secondary creep. Even so, in the C^* regime, for short cracks, Riedel and Detampel [8] observed deviations from the correlation of $\dot{a}$ with C^*, and attributed them to crack tip blunting [13].

Since material creep strains require time to acquire non-zero values, the stress-state at the instant of loading is purely elastic. Thereafter, small scale creeping develops near the crack tip, and propagates with time more extensively into the uncracked ligament [1]. Two of the empirical approaches developed in the literature to account for the time-dependent evolution of the crack-tip stress fields are noted here. Saxena [14] and Bassani et al. [15] proposed the load parameter C_t, which interpolated between the stress-state corresponding to small-scale yielding and extensive yielding. A simpler closed form time-dependent parameter, $C(t)$, was given by Ehlers and Riedel [16]. Both time-dependent load parameters approach C^* in the limit of long times.

Crack tip stress fields ahead of a stationary crack in a power law creeping material are investigated in the present work. It is convenient to identify a characteristic time, t_1, originally proposed by Riedel and Rice [17], which defines the transition from small scale-creep to extensive creep regimes. A novel finding is that for times $0 \leq t \leq t_1$, the opening stress computed using the finite element method is non-monotonic, and differs qualitatively from the monotonically decreasing load parameter based stress-fields. Such a decrease was termed 'self similar' by Riedel and Rice [17]. The effect of this discrepancy on the time to failure of material points ahead of the crack tip is also investigated. Different process zone sizes are simulated numerically by tuning the value of a damage parameter in a Kachanov-Rabotnov damage model. A key conclusion is that except in materials with very small process zones, the finite element model predicted times to failure differ substantially from those predicted by the load parameter based fields.

2. Constitutive Law And Damage Model

2.1. Norton's Power Law

Norton's power law [18] relates the inelastic strain rate $\dot{\varepsilon}^{\text{ie}}_{ij}$ to stress in the secondary creep regime as:

$$\dot{\varepsilon}^{\text{ie}}_{ij} = (3/2)B\sigma_e^{n-1}S_{ij}, \tag{1}$$

where, $\sigma_e = (3S_{ij}S_{ij}/2)^{1/2}$, and S_{ij} denotes the deviatoric stress. The constants B and n in Eq. (1) are experimentally determined from uniaxial creep tests after the onset of secondary creep. In uniaxial tension, $S_{11} = 2\sigma/3$, $S_{22} = S_{33} = -\sigma/3$, and $S_{12} = S_{13} = S_{23} = 0$. $S_{ij}S_{ij} = 2\sigma/3$, and Eq. (1) reduces to

$$\dot{\varepsilon}^{\text{ie}}_{11} = B\sigma^n. \tag{2}$$

2.2. Short And Long Time Limits

Instantaneously after load application, the stress state in the specimen is identical to that given by linear elasticity [1]. At this instant, the crack tip stress fields are completely characterised by the linear elastic stress intensity factor, K [19]. With time, creep deformation develops to relax the near crack tip stresses. At long times, the stress fields approach a steady-state, given by the Hutchinson-Rice-Rosengren field.

$$\sigma_{ij} = \left(\frac{C^*}{I_n\ B\ r}\right)^{1/(n+1)} \tilde{\sigma}_{ij}(\theta). \tag{3}$$

Here, r denotes the distance from the crack tip, and I_n a parameter dependent only on n. The intensity of this field is characterised by the C^* parameter. Expressions for K and C^* for compact tension specimens based on their geometry and material properties are given by Tada et al. [19] and Shih et al.[20], respectively.

Using dimensional considerations, Riedel and Rice [17], proposed that soon after the instant of load application, the stresses on the crack plane will decay following $\sigma_{ij} \sim 1/(EBt)^{1/(n-1)}$. Here, E denotes Young's modulus. Equating this 'self-similarly' decaying stress field to the long time C^* field, they obtained a characteristic time t_1, given by

$$t_1 = K^2(1-\nu^2)/[(n+1)EC^*]. \tag{4}$$

They suggested that self-similarly decaying stresses prevail ahead of the crack tip up to time t_1. For time $t > t_1$, they proposed assuming the time independent C^* field ahead of the crack tip. A more refined formula is due to Ehlers and Riedel [16]. Using empirical correlations against finite element results, they showed that the formulas

$$C(t) = C^*(1 + t_1/t), \tag{5}$$

and

$$\sigma_{ij}(r,t) = \left(\frac{C(t)}{I_n\ B\ r}\right)^{1/(n+1)} \tilde{\sigma}_{ij}(\theta) \tag{6}$$

capture the time dependence of the stress fields ahead of the crack tip very well.

2.3. Damage Model

A simple and widely used expression for the damage evolution [1] of the Kachanov-Rabotnov type is presently adopted:

$$\frac{d\omega}{dt}(r,t) = \frac{D\sigma_{nn}^{\chi}(r,t)}{(1+\phi)(1-\omega)^{\phi}}. \tag{7}$$

σ_{nn} denotes the opening component of stress acting normal to the fracture plane. The damage variable ω evolves toward 1 under the applied stress. However, ω does not correspond to a physically measurable quantity. r denotes the distance from the stationary crack tip. Integrating Eq. (7) at a fixed r yields

$$\int_0^t \sigma_{22}^{\chi}(r,\tau)d\tau = \frac{1}{D}[(1-\omega_1)^{1+\phi} - (1-\omega_2)^{1+\phi}]. \tag{8}$$

Letting $\omega_1 = 0$ and $\omega_2 = 1$ and correspondingly letting $t = t_{\mathrm{f}}$, where t_{f} specifies the time to failure of the material point r ahead of the crack tip yields:

$$\int_0^{t_{\mathrm{f}}(r)} \sigma_{22}^{\chi}(r,\tau)d\tau = \frac{1}{D}. \tag{9}$$

For a given spatiotemporal variation of opening stress $\sigma_{nn}(r,t)$, Eq. (9) identifies $t_{\rm f}(r)$.

Damage evolution based on Eq. (7) leads to mesh-dependence of the numerical results [21]. An alternative inelastic strain based damage evolution law, due to Nikbin et al. [22], states:

$$\frac{d\omega}{dt} = \frac{\dot{\varepsilon}^{\rm ie}_{nn}}{\varepsilon_{\rm f}}, \tag{10}$$

where $\varepsilon_{\rm f}$ denotes the limiting creep strain, or creep ductility of the material. $\varepsilon_{\rm f}$ also depends on the creep exponent and triaxiality. Again, ω evolves with deformation from 0 to 1; local failure is implied when $\omega = 1$. Integrating Eq. (10) in time, the local failure criterion is obtained as

$$\varepsilon^{\rm ie}_{nn}(t_{\rm f}) = \varepsilon_{\rm f}. \tag{11}$$

Material continuity ahead of the crack-tip breaks down due to the formation of significant damage in so-called process zones. Smaller values of D or $1/\varepsilon_{\rm f}$ correspond to smaller process-zones. While the present finite-element simulations take no account of the break-down of material continuity, the interpretation of these parameters in terms of process-zone sizes proves useful in interpreting predictions.

3. Results

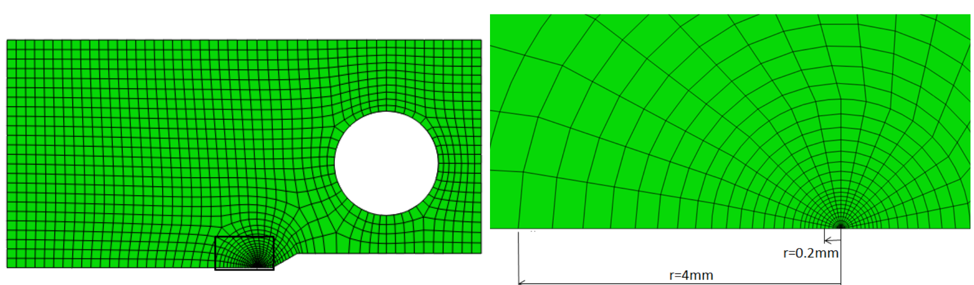

(a)

(b)

Figure 1: Finite element (a) specimen and (b) crack-tip meshes. Specimen geometry and loading is identical to that of specimen #10 of Maas and Pineau [9].

Simulations are performed on a compact tension specimen, whose geometry and loading are exactly identical to that of compact tension specimen #10 in the experimental study of Maas and Pineau [9]. The specimen and near-crack tip mesh are shown in Fig. 1. The ratio of the crack length to total length in this specimen is 0.34, and the specimen is crept at an applied load of 12070 N. Plane strain conditions are assumed. Large deformations are accounted for.

The material parameters assumed correspond to 2¼ Cr-1 Mo steel, given by Robinson [23]: $\mu_0 = 3 \times 10^7$ MPa h, $H = 0.001$ /h, $R = 0.0001$ /h, $k = 10$ MPa, $G_0 = 0.1$ MPa, and $n = 4$. Equivalent Norton law material parameters are determined by matching the secondary creep response of the Robinson material with Norton's material in uniaxial tension. It is determined that $B = 3.467 \times 10^{-14}$ MPa^{-n}/h and $n = 4$ in Eqs. (1) and (2). ABAQUS' in-built Norton law implementation is used. Also, following Riedel [1], it is assumed that the damage exponent $\chi = 6.2$ for 2¼ Cr-1 Mo steel.

For the present specimen, the mode I linear elastic stress intensity, as given by Tada et al. [19] works out to $K = 1189$ MPa $\sqrt{\text{mm}}$, and the steady state $C^* = 0.0532$ MPa mm/h according to Shih et al. [20]. Eq. (4) then yields $t_1 \approx 30$ h. The bulk of the time interval presently considered ($0 \leq t \leq 2000$ h) thus falls well within the ductile regime according to the criterion of Riedel and Rice [17].

3.1. Mechanical Fields

Let $\boldsymbol{n}$ be the normal to the crack plane. The spatiotemporal variation of the opening stress σ_{nn} predicted by various models is presented in Figs. 2 and 3. Figs. 2a and 2b show the time-independent short-time and long-time stress responses, as described in Sec. 2.2. These correspond to the stress states in the instant after load application and after an infinite time past load application, respectively.

Comparing the stress contours shown in Fig. 2a corresponding to the asymptotic K field given by Tada et al. [19] with those obtained from a finite element simulation assuming a linear elastic material (not shown), reveals that the re-

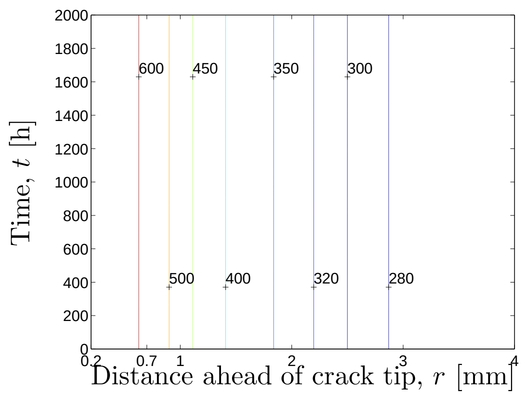

(a) Linear elastic

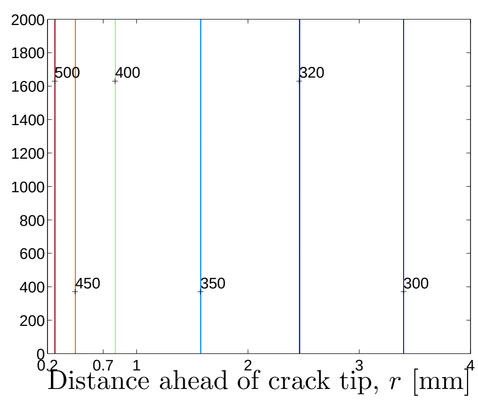

(b) C^* field

Figure 2: Spatiotemporal variation of stress σ_{nn} in the crack plane, as predicted by the: (a) K-field [19], and (b) C^*-field [20].

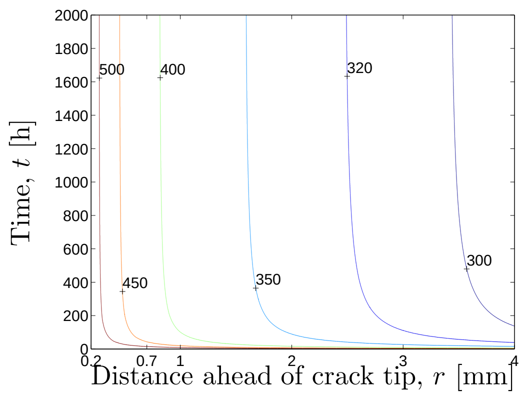

(a) Ehlers-Riedel $C(t)$-field

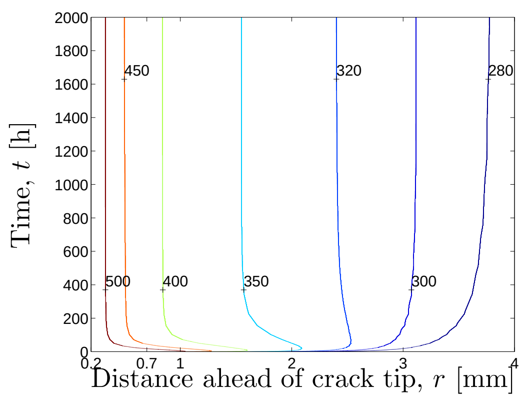

(b) Finite element implementing Norton's law

Figure 3: Spatiotemporal variation of stress σ_{nn} in the crack plane, as predicted by the: (a) $C(t)$-field [16], and (b) finite element implementing Norton's law [18].

gion of K-dominance is limited to 0 mm $\leq r \leq$ 2 mm. The steady-state asymptotic solution given by Shih et al. [20], plotted in Fig. 2b, is also accurate over 0 mm $\leq r \leq$ 2 mm. The spatiotemporal variation of the stress field given by Ehlers and Riedel [16] in Eq. (5) and (6) is shown in Fig. 3a. Finally, $\sigma_{nn}(r,t)$ predicted by the finite element analysis implementing Norton's law is shown in Fig. 3b. It is clear that the stresses predicted by the finite element simulations evolve from that predicted by the linear elastic model of Fig. 2a to that of the steady state solution shown in Fig. 2b at long times within the regime of validity of the K- and C^*-fields. It is also clear that in the K- and C^*-field dominant regimes, and in the regime corresponding approximately to $t > t_1$, the Ehlers-Riedel formula, Eq. (6), plotted in Fig. 3a closely matches that predicted by the finite element simulations, shown in Fig. 3b. Outside the region of dominance of the K and C^*-fields, however, the stress evolution is quite complex, as it is influenced by both specimen geometry and load distribution in the nett section.

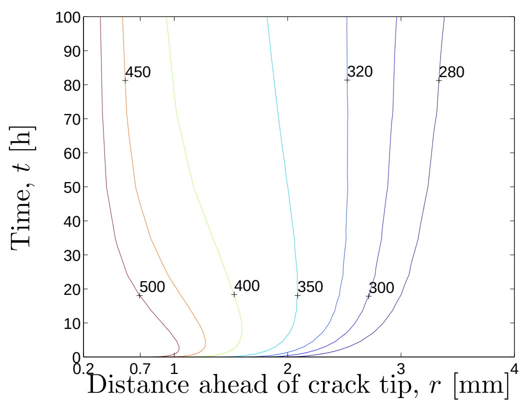

Figure 4: Spatiotemporal variation of stresses ahead of a stationary crack in the time interval 0 h$\leq t \leq$ 100 h revealing the non-monotonicity of normal stresses. This evolution is in contrast to the asymptotic monotonic decay proposed by Riedel and Rice [17].

In order to pay closer attention to the temporal regime $t < t_1$, a zoomed-in version of Fig. 3b focussing on the time interval 0 h $\leq t \leq$ 100 h is shown in Fig. 4. It is clear that material points ahead of the stationary crack experience non-monotonic variation of their stress state with time soon after loading, indeed over times $t \leq t_1$. The amplitude of the non-monotonic variation increases as the crack tip is approached. This is in contrast to the self-similar monotonic decrease of stress fields with time, $\sigma \sim 1/(EBt)^{1/(n-1)}$, assumed by Riedel and Rice [17]. To our knowledge, the break down of the self-similar time scaling of stress is reported here for the first time. In this regime, $t < t_1$, no agreement between the finite element calculated and the $C(t)$-based stress fields can be expected, as the latter strictly decay monotonically with time.

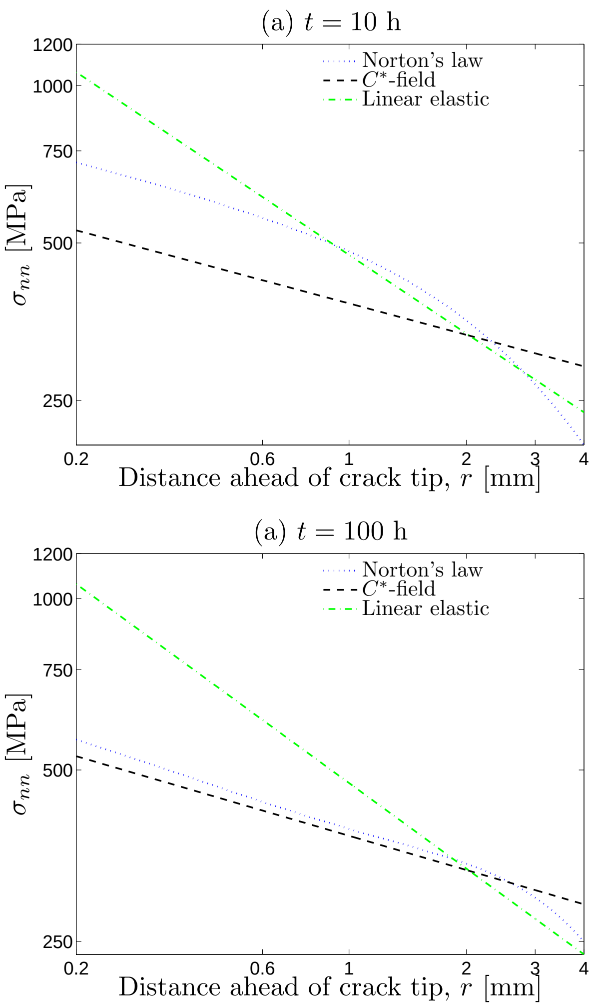

Figure 5: Stress field $\sigma_{nn}(r, t)$ ahead of the crack tip at (a) $t = 10$ h, and (b) $t = 100$ h. Note the logarithmic scaling of axes.

Fig. 5 shows the spatial distribution of stresses ahead of the crack at two fixed instants of time: $t = 10$ h$< t_1$, and $t = 100$ h$> t_1$. It is clear that the slope of the finite element predicted stress decay already matches that of the C^*-field at $t = 10$ h. The stress therefore decays as $\sim 1/r^{1/(n+1)}$ already at $t = 10$ h in accord with Eq. (6). Only the amplitude of stress intensity is greater. It is clear that the spatial distribution of stresses at this time is qualitatively more similar to the long-time limit than to the short-time limit, whereat the stress decay goes as $1/r^{1/2}$. The blunting with time of the singular stress field, from $\sim 1/r^{1/2}$ to $\sim 1/r^{1/(n+1)}$ will entail stress redistribution away from the crack tip. This redistribution appears to underlie the non-self similar temporal stress-decay observed in Fig. 4. At $t = 100$ h, the steady-state appears to have been nearly achieved and the stress field asymptotically near the crack tip is nearly equal to the C^*-field.

The spatiotemporal variation of the total (ε_{nn}) and creep (ε^c_{nn}) strains ahead of the finite element model crack tip are shown in Figs. 6a and 6b, respectively. The creep strains are smaller, but by no means negligible compared to the total strain. This shows that the specimen is undergoing extensive creep deformation by time $t = t_1$. According to Riedel and Rice [17], this means that C^* can be used as a load parameter at the crack tip. Furthermore, according to Riedel and Wagner [6], the present case must produce excellent correlations between C^* and crack growth rate $\dot{a}$, in contrast to the experimental observations of Maas and Pineau [9].

3.2. Time to Failure

The times to failure ahead of a stationary crack, t_{f}, given by Eqs. (9) and (11), as predicted by the finite element model are shown in Figs. 7 and 8, respectively. Also shown are the times to failure predicted assuming the C^* and $C(t)$ fields of Sec. 2.2.

In Fig. 7, the damage parameter D has been normalised by $D_0 = 1.425 \times 10^{-21}$ MPa$^{-\chi}$ /h, for convenience. For the smallest $D/D_0 = 1$ considered, the $C(t)$ predicted t_{f} matches the finite element predictions well. For larger values

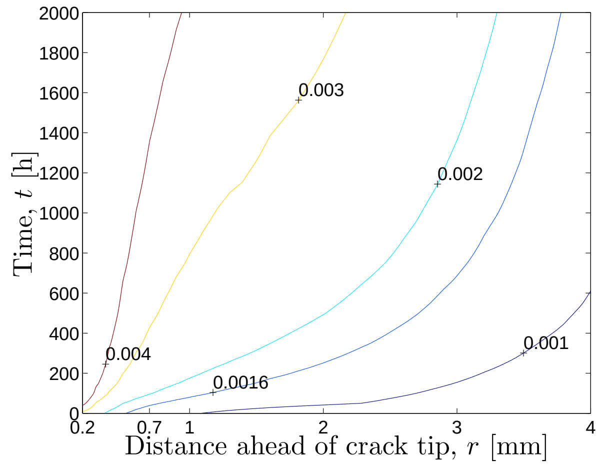

(a) Total strain

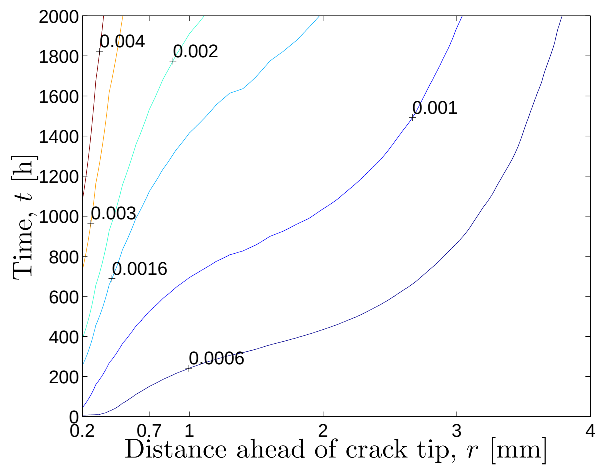

(b) Creep strain

Figure 6: Spatiotemporal variation of (a) total strain, ε_{nn} and (b) creep strain, ε^c_{nn} ahead of the crack tip predicted assuming Norton's law.

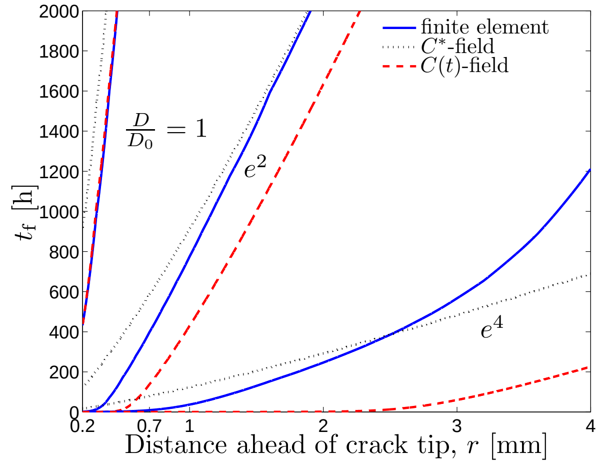

Figure 7: Spatiotemporal variation of time to failure t_f ahead of a stationary crack, following the stress-based damage model, Eq. (9).

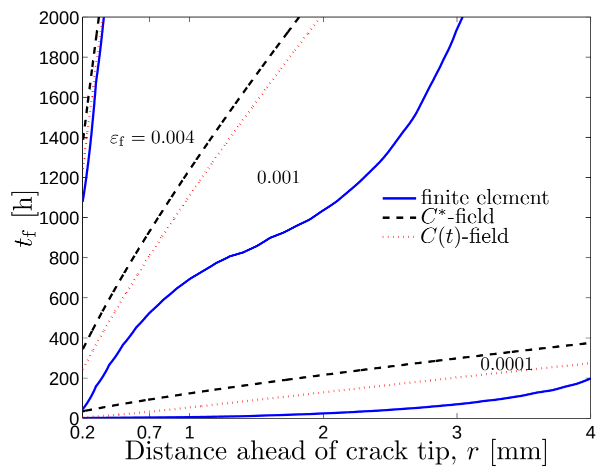

Figure 8: Spatiotemporal variation of time to failure t_f ahead of a stationary crack, following the inelastic strain-based damage model, Eq. (11).

of D/D_0, however, the agreement between the $C(t)$ field and finite element predicted t_f progressively worsens, even though the $C(t)$ field predicted t_f is always conservative. In all cases, the t_f predicted by the C^* field is a non-conservative over-estimate.

Similar observations and conclusions apply to the inelastic strain-based time to failure predictions shown in Fig. 8, provided D/D_0 is replaced by the reciprocal of the critical inelastic strain to failure, $1/\varepsilon_\mathrm{f}$. Again, reasonable agreement between the predicted times to failure using the finite element model, and the $C(t)$-field is obtained for small $1/\varepsilon_\mathrm{f}$, corresponding to the most localised damage ahead of the crack tip. More wide-spread damage corresponding to larger $1/\varepsilon_\mathrm{f}$ leads to dramatic disagreements, as shown. At $r = 1$ mm, which is well within the K-dominant zone, t_f obtained from the finite element fields, and from the $C(t)$ fields are 6 h, and 54 h, respectively for $\varepsilon_f = 0.0001$. The $C(t)$ fields thus overestimate t_f by almost a factor of 10. The relative disagreement is smaller with $\varepsilon_f = 0.001$. In this case, again at $r = 1$ mm, t_f obtained from the finite elements and $C(t)$ fields are 694 h, and 1110 h, which amounts to a ratio of about 2. Unlike in the stress-based model, predictions based on C^* and $C(t)$ do not bound the finite element results in the case of a creep-strain based damage criterion.

It is important to notice here that larger D or $1/\varepsilon_\mathrm{f}$ corresponds to larger process zones, i.e., ones that extend further ahead of the crack tip. Reasonable agreement between the finite element predictions of t_f with that based on $C(t)$ is only obtained in the case of highly localised damage ahead of the crack tip.

In creep ductile materials such as the present 2¼ Cr-1 Mo steel, significant damage occurs ahead of the crack tip. For this material, Riedel [1, p. 350] gives $D = 2.7 \times 10^{-17}$ MPa$^\chi$/h, which corresponds to $D/D_0 \approx e^{10}$ under conditions that were similar, but not identical to those of Mass and Pineau's [9] tests. The large value of D/D_0 suggests an extensive process zone. Furthermore, the large extent of the damage zone was experimentally verified by Bensussan et al. [10]. In light of the C^* or even the $C(t)$-based stress fields failing to be remain accurate over this extensive range, it is not surprising that the C^* does not correlate with the crack propagation rate, as observed experimentally [9, 10].

Since the deviations between the finite element predicted stresses and those obtained from $C(t)$ or C^*-fields is largest at times $t \leq t_1$, it is interesting to compare the damage state obtained from these models at time $t = t_1$. This is shown in Fig. 9. Corresponding to the stress-based damage model, Fig. 9a shows that the damage state at $t = t_1$ predicted by the $C(t)$ field is significantly larger than that predicted by the finite element field. The opposite is true for the strain-based damage model, with the finite element field predicting considerably more creep strain than the $C(t)$ field, as shown in Fig. 9b. It must be emphasised that these differences will persistently be carried forward even for $t > t_1$, even though in the latter regime, the finite element predicted stresses are in much better agreement with the $C(t)$-based stress fields, as shown previously in Sec. 3.1. In other words, the disagreement between the damage states predicted based on the finite element, and the $C(t)$ fields will not diminish in the time regime, $t > t_1$.

4. Discussion

It has been shown by means of a finite element calculation that the stress-state ahead of stationary crack-tip does not decay with time in a self-similar manner, as assumed by Riedel and Rice [17]. Material points in the K- or C^*-dominant zone experience a non-monotonic stress field, with the amplitude of the opening stress fluctuation increasing with approach to the crack-tip. This happens soon after specimen loading, within the time interval $t \leq t_1$, where t_1 is the characteristic time to transition from small scale creeping to extensive creeping in the specimen.

This observation has consequences for creep crack growth predictions, which are now enumerated. First, the crack-tip field is often obtained by interpolation between the small scale creeping field and the long-term C^*-field, e.g., Bassani et al. [15]. The present result suggests that such interpolation may be invalid as interpolation can only yield opening stresses that are monotonically decreasing in time. Furthermore, any correlations obtained between crack speed and the

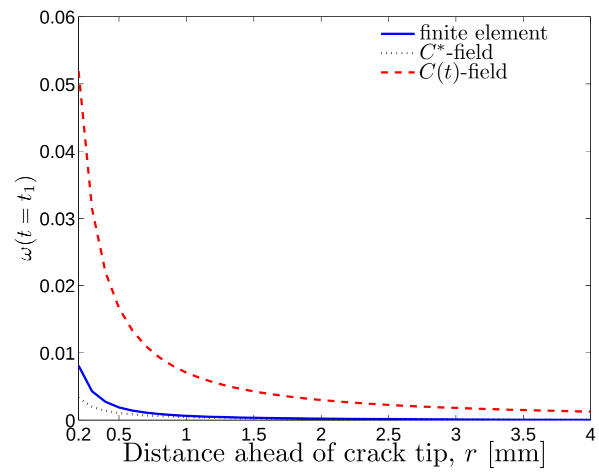

(a)

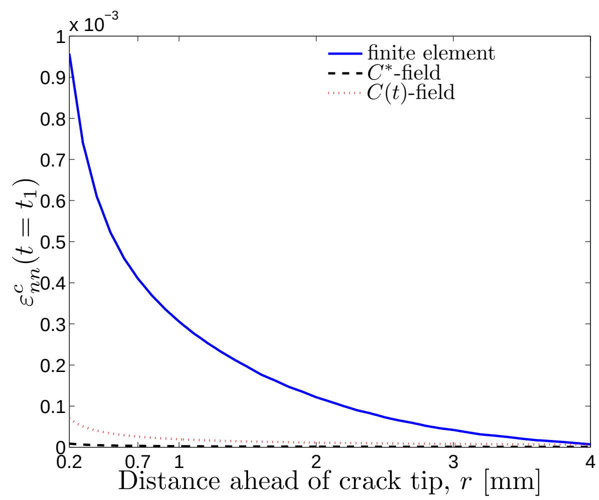

(b)

Figure 9: Damage predicted ahead of the crack at time $t = t_1$ by (a) the stress-based model, assuming $D/D_0 = 1$, and (b) the creep strain-based damage models.

interpolated load parameter may be coincidental. Second, nucleation of creep voids in the crack plane is a precursor for creep crack growth. This process is very sensitive to the crack plane opening stress [5]. Since the finite element predicted peak opening stress is greater in general than that predicted by the C^* or $C(t)$ fields, rapider creep void nucleation can generally be expected under the former field than the latter. Third, the rates of damage processes within the process zone, modelled assuming the asymptotic validity of the C^* or $C(t)$ fields, are most likely erroneous. This is because they do not accurately account for the damage evolution within the time $t \leq t_1$. The prediction error in the damage field carries over beyond $t = t_1$, as damage accumulation is cumulative. In short, inaccuracies associated with the load parameter based stress fields appear to be significant enough to significantly degrade the accuracy of any creep crack growth models based upon them, e.g., [6, 5, 24]. It is therefore scarcely surprising that model correlations between crack growth rates and load parameters, discussed in Sec. 1, are often found violated.

5. Conclusions

In a pioneering paper analysing the stress field ahead of a creep crack, Riedel and Rice [17] assumed that the stress state decays in a self-similar manner soon after loading. Based on this assumption, and dimensional analysis, they suggested that the stress scales as $\sim t^{1/(n-1)}$, where t denotes time, and n is the creep exponent. Using finite element analysis, the present work has shown that the assumption of self-similar decay does not hold. The stress-state at a typical material point ahead of the stationary crack increases with time before decreasing, as the load distribution ahead of the crack tip goes from the sharper $1/r^{1/2}$ elastic singularity to the blunter $1/r^{1/(n+1)}$ HRR singularity. Temporally, this transition spans the time period $0 \leq t \leq t_1$, where, t_1 is the characteristic time at which the small scale creeping at the crack tip may be regarded to transition to extensive creeping, following Riedel and Rice [17]. Since creep void nucleation and growth are highly sensitive to stress, these observations imply that load parameter based stress fields may not be suitable for predicting creep crack growth.

[1] H. Riedel, Fracture at high temperatures, Materials research and engineering, Springer-Verlag, Berlin, 1987.

[2] K. Shiro, O. Kiyotsugu, O. Keiji, An analysis of creep crack propagation on the basis of the plastic singular stress field, Eng. Fracture Mech. 11 (2) (1979) 315–329.

[3] J. Hutchinson, Singular behaviour at the end of a tensile crack in a hardening material, J. Mech. Phys. Solids 16 (1) (1968) 13–31.

[4] J. Rice, G. Rosengren, Plane strain deformation near a crack tip in a power-law hardening material, J. Mech. Phys. Solids 16 (1) (1968) 1–12.

[5] C. Y. Hui, V. Banthia, The extension of cracks at high temperature by growth and coalescence of voids, Int. J. Fracture 25 (1) (1984) 53–67.

[6] H. Riedel, W. Wagner, The growth of macroscopic cracks in creeping materials, in: D. F. et al. (Ed.), Advances in fracture research. Proc. fifth international conference on fracture, 683–690, 1981.

[7] H. Riedel, W. Wagner, Creep Crack Growth in Nimonic 80A and in a Cr-Mo Steel, in: S. R. V. et al. (Ed.), Advances in fracture research. Proc. sixth international conference on fracture, vol. 3, 2199–2206, 1984.

[8] H. Riedel, V. Detampel, Creep crack growth in ductile, creep-resistant steels, Int. J. Fracture 33 (4) (1987) 239–262.

[9] E. Maas, A. Pineau, Creep crack growth behavior of type 316L steel, Eng. Fract. Mech. 22 (2) (1985) 307–325.

[10] P. Bensussan, E. Maas, R. Pelloux, A. Pineau, Creep crack initiation and propagation: fracture mechanics and local approach, J. Pressure Vessel Tech. 110 (1) (1988) 42–50.

[11] R. Piques, P. Bensussan, A. Pineau, Application of fracture mechanics and local approach to creep crack initiation and growth, in: ECF6, Amsterdam 1986, 91–100, 2013.

[12] H. Riedel, Creep deformation at crack tips in elastic-viscoplastic solids, J. Mech. Phys. Solids 29 (1) (1981) 35–49.

[13] H. Riedel, Creep crack growth, in: R. P. Wei, R. P. Gangloff (Eds.), Fracture Mechanics: Perspectives and Directions, vol. ASTM STP 1020, ASTM, Philadephia, 101–126, 1989.

[14] A. Saxena, Creep crack growth under non-steady-state conditions, in: Fracture Mechanics: Seventeenth Volume, ASTM International, 185–201, 1986.

[15] J. L. Bassani, D. E. Hawk, A. Saxena, Evaluation of the Ct parameter for characterizing creep crack growth rate in the transient regime, in: Nonlinear Fracture Mechanics: Volume I Time-Dependent Fracture, ASTM International, 7–26, 1988.

[16] R. Ehlers, H. Riedel, A finite element analysis of creep deformation in a specimen containing macroscopic crack, in: ICF5, Cannes (France), 691–698, 1981.

[17] H. Riedel, J. R. Rice, Tensile cracks in creeping solids, in: Fracture Mechanics: 12th Conference, ASTM International, 112, 1980.

[18] F. H. Norton, Creep of steel at high temperatures, McGraw Hill, 1929.

[19] H. Tada, P. C. Paris, G. R. Irwin, The Stress Analysis of Cracks Handbook. The American Society of Mechanical Engineers, New York .

[20] C. Shih, V. Kumar, M. German, An engineering approach for elastic-plastic fracture analysis, EPRI NP-1931, RP1237-1 (July 1981) .

[21] S. Murakami, Y. Liu, M. Mizuno, Computational methods for creep fracture analysis by damage mechanics, Comput. Method. Appl. M. 183 (1) (2000) 15–33.

[22] K. Nikbin, D. Smith, G. Webster, Prediction of creep crack growth from uniaxial creep data, Proc. R. Soc. Lond. A. 396 (1810) (1984) 183–197.

[23] D. N. Robinson, A Unified Creep-Plasticity Model for Structural Metals at High Temperature, Tech. Rep. ORNL/TM-5969, Oak Ridge National Laboratory, 1978.

[24] J. L. Bassani, D. E. Hawk, Influence of damage on crack-tip fields under small-scale-creep conditions, International Journal of Fracture 42 (2) (1990) 157–172.